Am J Physiol Lung Cell Mol Physiol 316: L936–L945, 2019.
First published February 20, 2019; doi:10.1152/ajplung.00504.2018.

RESEARCH ARTICLE | *Translational Physiology*

Erythropoietin inhalation enhances adult canine alveolar-capillary formation following pneumonectomy

D. Merrill Dane,[1] Cuneyt Yilmaz,[1] Dipendra Gyawali,[1] Roshni Iyer,[1] Jyothi Menon,[3] Kytai T. Nguyen,[3] Priya Ravikumar,[1] Aaron S. Estrera,[2] and Connie C. W. Hsia[1]

[1]*Department of Internal Medicine, University of Texas Southwestern Medical Center, Dallas, Texas;* [2]*Department of Cardiothoracic Surgery, University of Texas Southwestern Medical Center, Dallas, Texas; and* [3]*Department of Bioengineering, University of Texas at Arlington, Arlington, Texas*

Submitted 14 November 2018; accepted in final form 13 February 2019

Dane DM, Yilmaz C, Gyawali D, Iyer R, Menon J, Nguyen KT, Ravikumar P, Estrera AS, Hsia CCW. Erythropoietin inhalation enhances adult canine alveolar-capillary formation following pneumonectomy. *Am J Physiol Lung Cell Mol Physiol* 316: L936–L945, 2019. First published February 20, 2019; doi:10.1152/ajplung.00504.2018.—Paracrine erythropoietin (EPO) signaling in the lung recruits endothelial progenitor cells, promotes cell maturation and angiogenesis, and is upregulated during canine postpneumonectomy (PNX) compensatory lung growth. To determine whether inhalational delivery of exogenous EPO augments endogenous post-PNX lung growth, adult canines underwent right PNX and received, via a permanent tracheal stoma, weekly nebulization of recombinant human EPO-containing nanoparticles or empty nanoparticles (control) for 16 wk. Lung function was assessed under anesthesia pre- and post-PNX. The remaining lobes were fixed for detailed morphometric analysis. Compared with control treatment, EPO delivery significantly increased serum EPO concentration without altering systemic hematocrit or hemoglobin concentration and abrogated post-PNX lipid oxidative stress damage. EPO delivery modestly increased post-PNX volume densities of the alveolar septum per unit of lung volume and type II epithelium and endothelium per unit of septal tissue volume in selected lobes. EPO delivery also augmented the post-PNX increase in alveolar double-capillary profiles, a marker of intussusceptive capillary formation, in all remaining lobes. EPO treatment did not significantly alter absolute resting lung volumes, lung and membrane diffusing capacities, alveolar-capillary blood volume, pulmonary blood flow, lung compliance, or extravascular alveolar tissue volumes or surface areas. Results established the feasibility of chronic inhalational delivery of growth-modifying biologics in a large animal model. Exogenous EPO selectively enhanced cytoprotection and alveolar angiogenesis in remaining lobes but not whole-lung extravascular tissue growth or resting function; the nonuniform response contributes to structure-function discrepancy, a major challenge for interventions aimed at amplifying the innate potential for compensatory lung growth.

alveolar angiogenesis; canine model; intussusceptive capillary formation; lung diffusing capacity; morphometry; oxidative stress

INTRODUCTION

Extensive investigation has shown that, following unilateral pneumonectomy (PNX) in adult canines, the remaining lung undergoes compensatory lung growth followed by architectural remodeling that eventually enhance the function of the remaining lung (7, 8, 32, 33). These highly coordinated adaptive events are mediated by myriad homeostatic metabolic pathways, including paracrine erythropoietin (EPO) signaling via its receptor (EPOR) (9, 45–47). In addition to stimulating proliferation and differentiation of erythroid progenitor cells in the bone marrow (35), the EPO-EPOR axis is active in many extrahematopoietic tissue, including the lung (9). Paracrine/autocrine EPO-EPOR signaling has been implicated in wide-ranging homeostatic functions, including organogenesis, cell proliferation, antiapoptosis, cytoprotection, recruitment of endothelial progenitor cells, and proangiogenesis (18, 26). Both EPO-EPOR and vascular endothelial growth factor (VEGF) are downstream effectors of transcriptional regulation by hypoxia inducible factor-1α (HIF-1α) (45). The angiogenic potency of EPO has been reported to equal that of VEGF (17). We observed upregulation of HIF-1α-EPOR-VEGF axis in the remaining lung of adult canines following right PNX (resection of ~58% of lung units), suggesting that this axis plays a role in mediating reinitiation of compensatory lung growth and/or remodeling (9, 45–47). Furthermore, HIF-1α may be activated by not only hypoxia but also mechanical stress (4, 28); the latter has emerged as the predominant in vivo stimulus for post-PNX compensatory lung growth (11).

On the basis of the above observations, we hypothesized that enhancing EPO-EPOR signaling in the lung via targeted delivery of exogenous EPO augments endogenous post-PNX lung growth. To minimize dose requirement in chronic administration, we incorporated recombinant human EPO within biocompatible, biodegradable polymeric nanoparticles for improved cell uptake, sustained release, and induced action (25). To minimize off-target bone marrow erythropoiesis associated with systemic EPO delivery, the EPO-containing nanoparticles were nebulized for inhalational delivery to the lung (31) via a permanent tracheal stoma in canines following right PNX. Matched control animals received empty nanoparticles in the same manner. Here, we report the results of physiologic measurements and postmortem morphometry. In vivo imaging using volumetric computed tomography was also performed at two transpulmonary pressures for separate detailed parenchymal deformation analysis.

Address for reprint requests and other correspondence: C. C. W. Hsia, Pulmonary & Critical Care Medicine, Dept. of Internal Medicine, Univ. of Texas Southwestern Medical Center, 5323 Harry Hines Blvd., Dallas, TX 75390-9034 (e-mail: connie.hsia@utsouthwestern.edu).

1040-0605/19 Copyright © 2019 the American Physiological Society

Downloaded from journals.physiology.org/journal/ajplung (193.140.001.200) on February 25, 2022.

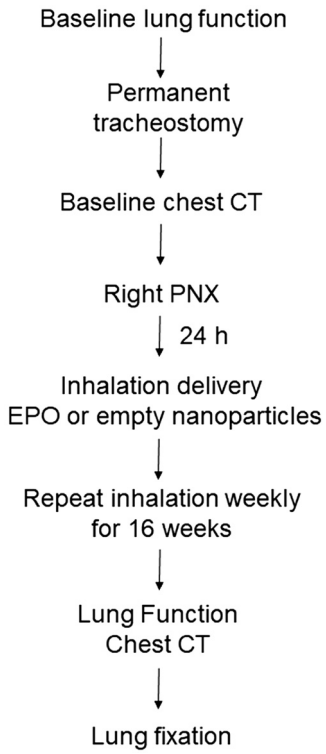


Fig. 1. Time line of studies. CT, high resolution chest computed tomography; EPO, erythropoietin; PNX, pneumonectomy.

METHODS

Animals and experiments. The Institutional Animal Care and Use Committee of the University of Texas Southwestern Medical Center approved all procedures. Adult litter-matched mixed-breed male hounds ($n = 4$ per treatment group, total $n = 8$), 10–11 mo old at time of surgery, and body weight 25.1 ± 3.4 kg (mean ± SD) were obtained from an approved vendor. The experimental timeline and studies are shown in Fig. 1.

Permanent tracheal stoma. We used the procedure of Bartoli et al. (2). The animal was fasted, premedicated with injections of acepromazine (0.05 mg/kg im), atropine (0.04 mg/kg im), buprenorphine (0.01 mg/kg im), cefazolin (22 mg/kg iv), and carprofen (4.4 mg/kg sc). Anesthesia was induced using propofol (4 mg/kg iv) and maintained using isoflurane. Animals were intubated and mechanically ventilated. The neck was shaved and prepared with Betadine and alcohol scrub. In a sterile manner and via a midline neck incision, the trachea was exposed and the sternohyoid muscles divided down the midline. Prolene sutures were used to fix the divided sternohyoid muscle to the lateral trachea. The trachea was opened at the second ring. Anterior portions of the second, third, and fourth rings were removed to create a 2 × 1-cm opening in the tracheal wall. The skin flaps were elevated and a 1.0- to 1.5-cm ellipse of skin was removed from either side of the tracheal opening. The incision was closed above and below the stoma and secured to the tracheal mucosa at the edges of the stoma. Nonabsorbable monofilament sutures were used to secure the skin in direct apposition to the incised tracheal cartilage so that the sternohyoid muscles and the exposed tracheal cartilage were covered with ventral neck skin. The skin above and below the stoma were loosely opposed with continuous Vicryl suture. Postoperative analgesia with buprenorphine was administered for 48 h. The neck was bandaged and the stoma examined and cleaned at regular intervals. Sutures were removed 14 days after surgery. Wound healing was complete by 3–4 wk. Animals could breathe through the stoma or upper airway and could bark normally. Once healed, the stoma was low maintenance, permitting repeated intubation, respiratory studies, and aerosol nebulization.

Right pneumonectomy. After healing of tracheal stoma and completion of pre-PNX measurements, the animal underwent right PNX following established procedures (8). Briefly, the animal was anesthetized, intubated, and mechanically ventilated. Rectal temperature, heart rate, blood pressure, and transcutaneous O_2 saturation were continuously monitored. A right lateral thoracotomy was performed in the fifth intercostal space. Lobar vessels were ligated and cut. The bronchi were stapled and the right lung removed. The bronchial stump was immersed in warm saline to check for leaks and then over-sewn with loose hilar tissue for added protection. Lidocaine (1%) was applied to the intercostal nerves. The chest wall was closed in layers. Residual thoracic air was evacuated to underwater seal. Supplemental O_2 was administered as needed. Blood loss was minimal. Intraoperative fluid administration was minimal (<50 ml). Buprenorphine was administered postoperatively for 48 h and as needed thereafter. Skin stitches were removed after 7–10 days.

EPO nanoparticles. Using an emulsion-solvent evaporation technique, poly-lactic-co-glycolic acid (PLGA, Lakeshore Biomaterial, Birmingham, AL) nanoparticles (average diameter 180 nm) were loaded with recombinant human EPO (cat. no. CRE-600C, Cell Sciences, Canton, MA); bovine serum albumin was added as a cryoprotectant and enhancer of EPO bioactivity, which was measured as the ability to maintain the viability of EPOR-expressing BaF3 cells (gift from Lily Huang, Dept. of Cell Biology, University of Texas Southwestern) (Fig. 2). Physical properties of the nanoparticles have been characterized previously (25).

Inhalational delivery. Animals underwent nebulization of the test compounds 1 day after PNX and weekly thereafter for 16 wk. For this procedure, the animal was sedated with atropine (0.04 mg/kg im) and diazepam or midazolam (0.2 mg/kg im) with butorphanol (0.2 mg/kg im) added as needed to prevent agitation. While partially restrained standing in a sling, local anesthesia (lidocaine 1%) was applied to the tracheal stoma. An endotracheal tube was inserted and the cuff inflated. PLGA nanoparticles (0.5 mg/kg) loaded with recombinant human EPO (100 units/kg) were suspended in sterile PBS (5 ml), sonicated for 2 min, nebulized (Pulmomate Model 4650D; Devilbiss Health Care, Somerset, PA, average droplet size 2.7 μm), and delivered into the tracheal tube. Exhaled air was collected via a respiratory mask into a reservoir bag and recirculated in a closed circuit to maximize delivery. Oxygen concentration in the rebreathing system

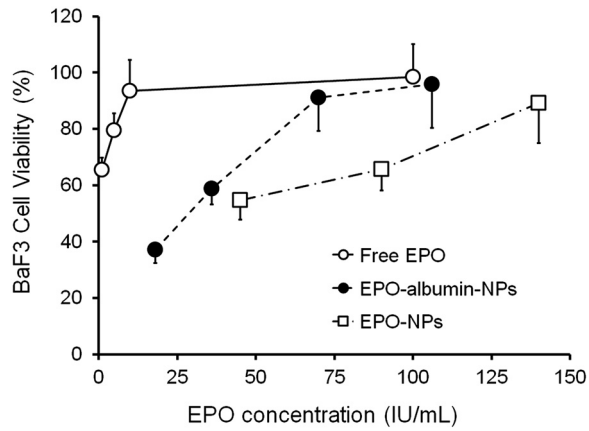


Fig. 2. Bioactivity of erythropoietin (EPO)-containing poly-lactic-co-glycolic acid (PLGA) nanoparticles (NPs) was tested using EPO receptor (EPOR)-expressing BaF3 cells that depend on the presence of EPO for survival. Compared with free EPO, EPO-containing NPs show reduced bioactivity in preserving BaF3 cell viability. Adding albumin as a cryoprotectant restored bioactivity of EPO NPs at EPO concentrations >75 IU/ml. Mean ± SD. Triplicate assays.

Downloaded from journals.physiology.org/journal/ajplung (193.140.001.200) on February 25, 2022.

was monitored and supplemental O_2 added to maintain the inspired O_2 concentration at ~21%. Complete nebulization occurred in ~15 min; expired CO_2 concentration remained under 5%. Control animals received empty nanoparticles in the same manner. Body weight, venous blood hematocrit, and hemoglobin concentration were measured weekly while conscious and standing at rest, and serum EPO concentration was measured every 4 wk. Four animals per treatment group were studied.

To verify inhalational EPO delivery to the lung, one additional animal received under anesthesia nebulized EPO (100 units/kg) conjugated to 5-carboxytetramethylrhodamine suspended in phosphate buffered saline (PBS; 5 ml) delivered via an endotracheal tube. Following EPO delivery, the animal was euthanized. The left lung was removed and fixed by tracheal instillation of 4% paraformaldehyde at 25 cmH_2O airway pressure. The fixed left caudal lobe was sectioned, and random samples were embedded in paraffin for fluorescent microscopy to visualize the inhaled EPO nanoparticles in lung parenchyma (Fig. 3*A*).

Blood assays. Following inhalation delivery, peripheral venous blood was drawn to monitor hematocrit and hemoglobin concentration. In addition, serum EPO concentration (Human Quantikine IVD ELISA kit, DEP00, R&D Systems, Minneapolis, MN) and markers for plasma lipid and DNA oxidative stress damage: 8-isoprostane (ELISA kit, Cayman Chemical, Ann Arbor, MI) and 8-hydroxy-2'-deoxyguanosine (Oxidative DNA Damage ELISA kit, Cell BioLabs, San Diego, CA) were measured pre-PNX and at selected time points post-PNX.

Physiological studies. Lung function was measured at baseline pre-PNX and following completion of post-PNX inhalation treatments. Animal was fasted overnight, premedicated with acepromazine (0.05 mg/kg im) and atropine (0.04 mg/kg im). Anesthesia was induced with propofol (4 mg/kg iv) and maintained with an intravenous infusion of ketamine and diazepam at a dose titrated to effect. Animals were intubated and mechanically ventilated in the supine position (tidal volume 10–12 ml/kg, 16–18 breaths per min) to eliminate spontaneous breathing effort. Rectal temperature, heart rate, and transcutaneous O_2 saturation were monitored. Mouth and esophageal pressures were measured using separate transducers. Static transpulmonary pressure (P_{tp})-lung volume (PV) curves were measured using a calibrated syringe inflating the lungs to 15, 30, 45, and 60 ml/kg above end-expiratory lung volume (EELV) or up to P_{tp} of 30 cm H_2O, in increasing and then decreasing order. End-inspiratory lung volume and EELV, pulmonary blood flow, diffusing capacity for lung and membrane, capillary blood volume, and septal tissue volume (including microvascular blood) were measured simultaneously using an established rebreathing technique (5, 6, 34) at two inspired oxygen tensions (21% and 99%) and two lung volumes (30 ml/kg and 45 ml/kg above EELV).

Duplicate measures under each condition were averaged. PV curves were analyzed using established methods (27, 36). Specific lung compliance was calculated from the changes in lung volume and P_{tp} from 10 to 30 cm H_2O and normalized by the lung volume at 10 cm H_2O.

Terminal procedure. Under deep anesthesia, a cuffed endotracheal tube was inserted into the tracheal stoma and tied securely. The abdomen was opened via a midline incision and the lung collapsed via a diaphragmatic incision. An overdose of pentobarbital and phenytoin was administered intravenously and the remaining lobes reinflated within the thorax by tracheal instillation of 2.5% buffered electron microscopy-grade glutaraldehyde at 25 cmH_2O of hydrostatic pressure above the sternum. After the flow of fixative ceased, the tracheal tube was closed to maintain airway pressure. The lungs were removed intact, immersed in buffered 2.5% glutaraldehyde, floated on a water bath, and stored at 4°C for at least 4 wk before further processing.

Lung morphometry. Volume of each intact lobe was measured by saline immersion, then the lobe serially sectioned (2-cm thickness). Volume of the sectioned lobe was measured by the Cavalieri Principle

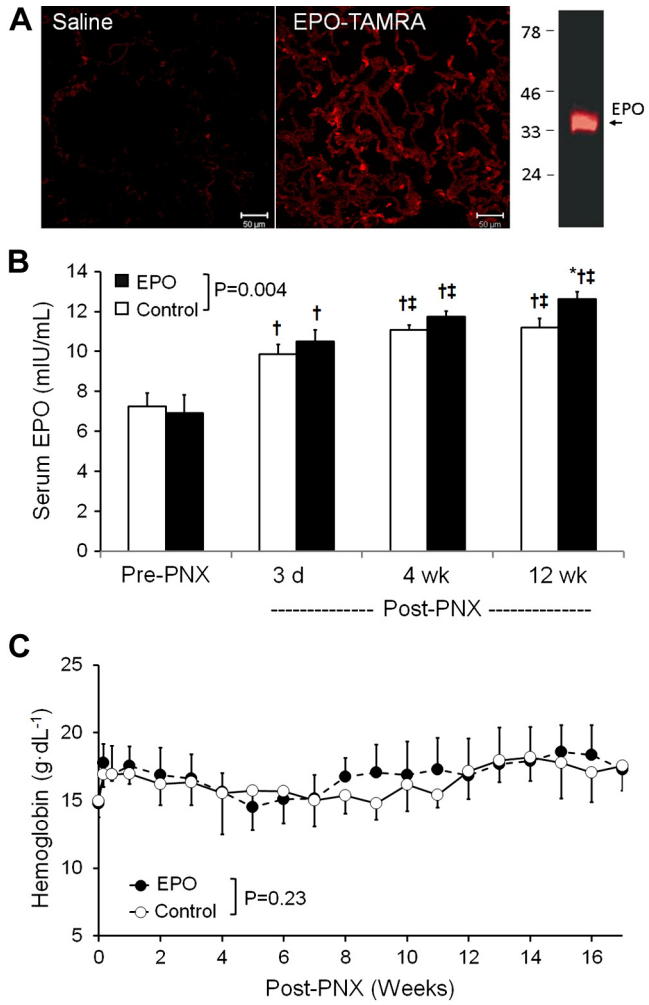


Fig. 3. Post-PNX inhalational delivery of recombinant EPO. *A*: EPO conjugated to 5-carboxytetramethylrhodamine (TAMRA; blot at right) was nebulized and delivered via endotracheal tube to one animal compared with a vehicle (saline)-treated control animal. *B*: serum EPO level increased following right PNX; the increase was accentuated in animal receiving EPO nanoparticles compared with control animals receiving empty nanoparticles. Mean ± SD. Four animals per group. $P < 0.005$: EPO versus control by repeated measures ANOVA with post hoc Fisher's protected least significant difference test. *$P < 0.05$ versus control; †$P < 0.05$ versus pre-PNX; ‡$P < 0.05$ versus 3 days post-PNX. *C*: systemic hemoglobin concentration did not differ between treatment groups ($P = 0.23$ by repeated measures ANOVA). EPO, erythropoietin; PNX, pneumonectomy.

(43). A systematic random sampling scheme was used to select four tissue blocks per lobe; these were subsampled to select two blocks per lobe (six blocks per lung) for further processing and analysis. Samples were postfixed (1% osmium tetroxide in 0.1 M cacodylate buffer), stained with 2% uranyl acetate, dehydrated through graded alcohol, and embedded in resin (Spurr, Electron Microscopy Sciences, Hartfield, PA).

A stratified scheme was used for analysis: low- and high-power light microscopy (LM; ×275 and ×550) and transmission electron microscopy (TEM; ~×19,000) (10, 13). For LM, each block was sectioned (1 μm) and stained (toluidine blue). One section per block was overlaid with a test grid. At ×275, ≥20 nonoverlapping microscopic fields/block were systematically sampled from a random start. Using point counting and excluding structures 20 μm to 1 mm in diameter, volume densities of fine parenchyma, acinar airways, and alveoli per unit lung volume were estimated. At ×550, ≥20 nonover-

Downloaded from journals.physiology.org/journal/ajplung (193.140.001.200) on February 25, 2022.

Table 1. *Lung function measured under anesthesia*

	Group and Time				*P* Value		
	Control		EPO				
	Pre-PNX	Post-PNX	Pre-PNX	Post-PNX	Group	Time	Group × Time
Body weight, kg	27.1 ± 2.8	24.7 ± 3.0	24.0 ± 3.4	24.1 ± 2.0	0.21	**0.006**	**0.003**
Hemoglobin, awake, g/dl	15.2 ± 1.7	14.9 ± 0.9	14.4 ± 1.4	15.1 ± 0.6	0.62	0.74	0.41
Hemoglobin, anesthetized, g/dl	12.2 ± 0.7	12.7 ± 0.5	12.1 ± 1.0	13.5 ± 0.9	0.23	**0.0007**	**0.05**
Specific lung compliance, ml·(cm H_2O·l)$^{-1}$	23.0 ± 2.6	24.9 ± 4.6	22.3 ± 1.7	22.2 ± 4.3	0.38	0.64	0.59
Rebreathing measurements							
Alveolar O_2 tension, mmHg	123 ± 9	123 ± 5	126 ± 3	124 ± 4	0.57	0.33	0.49
End-expiratory lung volume, ml/kg	29.2 ± 5.8	36.5 ± 7.9	35.1 ± 3.5	38.9 ± 8.1	0.19	**0.0004**	0.17
End-inspiratory lung volume, ml/kg	69.4 ± 3.9	75.9 ± 8.3	79.7 ± 4.0	78.4 ± 7.9	**0.02**	0.21	0.07
Pulmonary blood flow, ml·(min·kg)$^{-1}$	90.6 ± 13.5	91.3 ± 12.7	87.1 ± 6.9	89.3 ± 11.0	0.60	0.55	0.76
Septal tissue volume, ml/kg	6.58 ± 1.23	5.28 ± 0.79	6.53 ± 2.00	5.85 ± 2.22	0.57	0.18	0.67
DL_{CO}, ml·(min·mmHg·kg)$^{-1}$	0.72 ± 0.07	0.54 ± 0.07	0.72 ± 0.07	0.54 ± 0.02	0.93	**<0.0001**	0.98
DM_{CO}, ml·(min·mmHg·kg)$^{-1}$	1.38 ± 0.27	1.01 ± 0.23	1.27 ± 0.34	1.09 ± 0.16	0.92	**<0.001**	0.12
V_c, ml/kg	2.40 ± 0.55	1.85 ± 0.20	2.67 ± 0.31	1.66 ± 0.15	0.68	**<0.0001**	0.06

Values are means ± SD; 4 animals/group. Inflation volume at 30 ml/kg above end-expiratory lung volume. DL_{CO}, lung diffusing capacity, expressed at a standard alveolar P_{O_2} of 120 mmHg and hemoglobin concentration of 14.6 g/dl; DM_{CO}, membrane diffusing capacity; V_c, pulmonary capillary blood volume. Specific lung compliance was calculated from transpulmonary pressures between 10 and 30 cm H_2O. Repeated-measures ANOVA. *P* values <0.05 are shown in boldface.

lapping microscopic fields/block were systematically imaged to estimate volume density of alveolar septa. For TEM, the blocks were sectioned (70 nm) and mounted on copper grids. Each grid was examined at ~×19,000 (JEOL EXII). At least 30 nonoverlapping fields per grid were systematically sampled. Volume densities of epithelium (type I or II), interstitium, endothelium, and capillaries were estimated by point counting with alveolar septum as the reference space. Alveolar epithelial and capillary surface densities per unit septum were estimated by intersection counting. At least 300 points or intersections were counted per grid. The length of test lines that transect the tissue-plasma barrier to the nearest erythrocyte membrane were measured to calculate mean harmonic thickness of the tissue-plasma barrier (13).

Absolute volumes and surface areas of individual structures were calculated by relating the volume and surface densities through the levels to the lobar volume. Prevalence of double-capillary profiles, an index of intussusceptive capillary formation, was estimated by completely sampling two grids per lobe under TEM (×3,000) and the results expressed as a ratio of [double/(single +double)] capillary profiles.

Statistical analysis. Measurements were normalized by body weight where appropriate and expressed as mean ± SD. Differences between treatment groups were compared by factorial ANOVA. PV curves were analyzed by established methods (27, 36). Temporal changes and differences among lobes were compared between treatment groups by repeated measures ANOVA with post hoc Fisher's protected least significant difference test (STATVIEW v.5.0). A *P* value ≤0.05 was considered significant.

RESULTS

Systemic response. Animals tolerated PNX and inhalation treatment without complication. Post-PNX body weight decreased in the control group but was maintained in the EPO-treated group (Table 1). Serum EPO concentration increased modestly (6%–13%) post-PNX in both groups, becoming higher in EPO-treated than control animals (Fig. 3*B*). Circulating hemoglobin concentration measured while awake and standing was not significantly different pre- to posttreatment or between groups (Fig. 3*C*). Circulating hemoglobin measured under anesthesia increased modestly post-PNX in both groups; the increase was larger in the EPO-treated group (Table 1). Circulating hemoglobin concentration is typically higher in the conscious than the anesthetized state; the difference reflects erythrocytes sequestration in the spleen at rest and their release into circulation under sympathetic stimulation.

In control animals, plasma 8-isoprostane level increased nearly threefold 3 days post-PNX then gradually returned to baseline by 4 wk; EPO inhalation abolished the post-PNX increase in 8-isoprostane level (Fig. 4*A*). EPO inhalation had

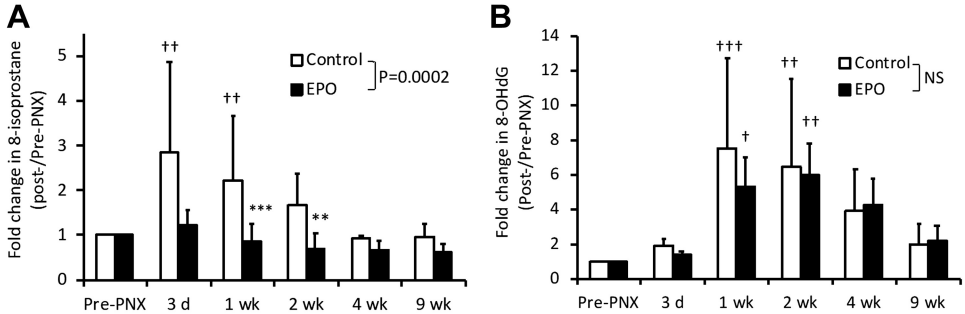


Fig. 4. Plasma 8-isoprostane (*A*) and 8-hydroxy-2′-deoxyguanosine (8-OHdG) (*B*) levels at pre-PNX and selected post-PNX time points. Mean ± SD. Four animals per group. *P* values for control versus EPO groups by repeated measures ANOVA are indicated. At each time point, EPO versus corresponding control: $^{**}P < 0.01$; $^{***}P < 0.001$. Post-PNX versus corresponding pre-PNX baseline: †$P < 0.05$; ††$P < 0.01$; †††$P < 0.001$. Repeated measures ANOVA and post hoc Fisher's protected least significant difference test. EPO, erythropoietin; PNX, pneumonectomy.

Downloaded from journals.physiology.org/journal/ajplung (193.140.001.200) on February 25, 2022.

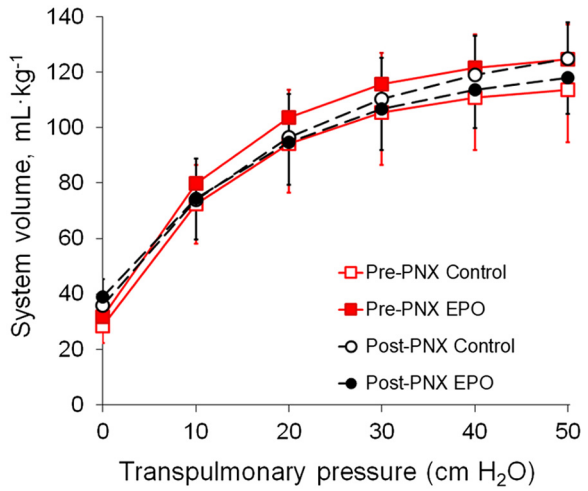


Fig. 5. Transpulmonary pressure-lung volume relationships measured pre- and post-PNX were not significantly different between control and EPO-treated animals. Mean ± SD. Four animals per group and time point. $P = 0.84$ by repeated measures ANOVA. EPO, erythropoietin; PNX, pneumonectomy.

no effect on post-PNX plasma 8-hydroxy-2'-deoxyguanosine level, which increased more slowly, peaking at 1 wk (Fig. 4*B*).

Lung function. Post-PNX lung volume at a given P_{tp} was not significantly different from that pre-PNX. The PV curves and specific lung compliance did not differ significantly between treatment groups (Fig. 5, Table 1). As expected, EELV was higher whereas diffusing capacity for lung, diffusing capacity for membrane, and capillary blood volume were lower post-PNX compared with pre-PNX; however, there were no significant differences in these measures between treatment groups (Table 1).

Lung morphometry. Following right PNX, 3 lobes of the left lung remained: cranial, middle, and caudal, comprising on average 12%, 7%, and 23%, respectively, of the original total units in both lungs (33). The left middle lobe is generally considered the inferior part of the left cranial lobe because its bronchus arises immediately next to that of the left cranial lobe (16). However, we have considered left middle as a separate lobe because its mechanical behavior and post-PNX adaptation often differ from that of the left cranial lobe (8).

Representative distal lung morphology was grossly similar between groups (Fig. 6). Fixed lobar volumes, morphometric alveolar-capillary hematocrit, and arithmetic mean septal thickness and harmonic mean barrier thickness were not different between groups (Table 2).

The coefficients of error for key primary measurements (volume densities of septal constituents) were ≤0.10. The coefficients of error for surface densities of alveoli and capillaries were ≤0.12. Alveolar septal volume density per unit of lung volume was higher in the EPO-treated group. Within the septa the volume density of alveolar type II epithelium and endothelium per unit of septum volume were higher in the EPO-treated group. Alveolar and capillary surface densities per unit of septum volume were not different between groups (Table 2). Heterogeneous responses were observed among the remaining lobes. In EPO-treated animals compared with controls, the ratio of alveolar septum volume per unit of lung volume was selectively elevated in the left middle lobe (Fig. 7*A*). Within the alveolar septum, the ratio of type II epithelium volume per unit of septal extravascular tissue volume was selectively elevated in the left caudal lobe (Fig. 7*B*). The ratio of endothelium volume per unit of septal extravascular tissue volume was higher in all remaining lobes (Fig. 7*C*). However, the above modestly and selectively higher ratios did not translate into significant increases in whole-lung average absolute volumes or surface areas of the major septal compartments (Table 3).

EPO-treated animals exhibited significantly elevated volume densities and absolute volumes of mitochondria within alveolar type II epithelium especially in the left caudal lobe (Fig. 8) and a marked increase in electron-dense inclusion bodies within interstitial cells of all remaining lobes; these circumscribed membrane-bound inclusion bodies are most likely ferritin-containing endosomes also visualized by Prussian Blue stain under stain under light microscopy (Fig. 9). EPO regulates iron metabolism in coordination with bone marrow erythropoiesis by increasing intestinal iron absorption, mobilizing iron stores for binding to transferrin and delivery to tissues where the iron is endocytosed and transported to intracellular sites such as mitochondria for heme synthesis or ferritin for storage (38). These interstitial cells are likely macrophages or histiocytes as EPO is known to mobilize iron from reticuloendothelial macrophages for recycling (23). Thus, inhalation of exogenous EPO effectively heightened cellular metabolic activity in the lung.

Right PNX consistently increased the prevalence of alveolar double-capillary profiles in all remaining lobes compared with unoperated normal adult canines previously studied using the same methods (33) (Fig. 10, $P = 0.0001$). EPO treatment modestly and significantly enhanced (by 12%–28%) the post-PNX increase in double capillary profiles in all remaining lobes compared with control treatment (Fig. 10, $P = 0.01$).

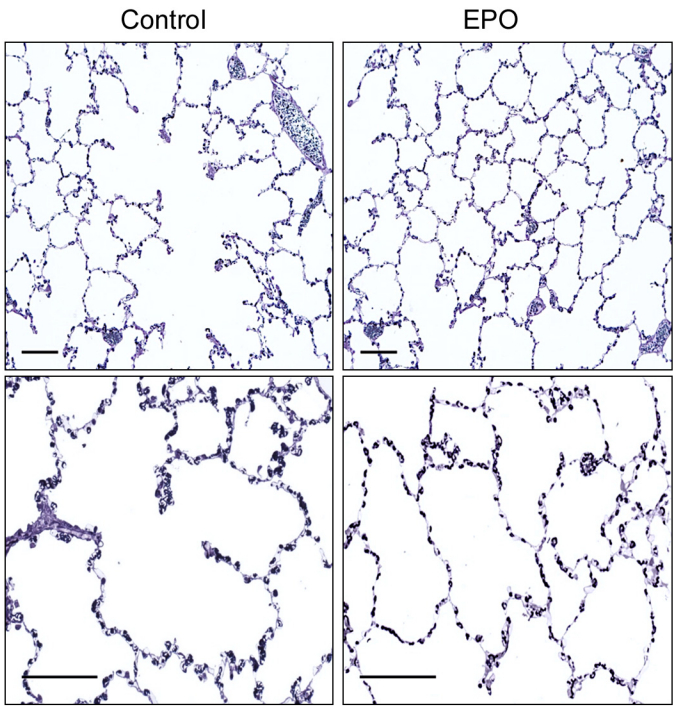


Fig. 6. Representative light micrographs of distal lung morphology at two magnifications in post-PNX animals treated with EPO or empty nanoparticles (control). Bar = 100 μm. EPO, erythropoietin; PNX, pneumonectomy.

Downloaded from journals.physiology.org/journal/ajplung (193.140.001.200) on February 25, 2022.

Table 2. *Morphometry: volume-to-volume and surface-to-volume ratios*

	Treatment		
	Control	EPO	*P* Value
Body weight, kg	24.7 ± 2.9	23.7 ± 2.3	0.34
Lung volume, ml			
Intact	1,333 ± 124	1,233 ± 211	0.44
After sectioning	1,180 ± 164	1,091 ± 229	0.55
Morphometric hematocrit	0.514 ± 0.009	0.503 ± 0.007	0.12
Arithmetic septal thickness, μm	5.19 ± 0.11	5.20 ± 0.11	0.87
Harmonic mean barrier thickness, μm	0.86 ± 0.02	0.87 ± 0.02	0.45
	Volume/volume ratio		
Coarse parenchyma/lung	0.9053 ± 0.0045	0.9031 ± 0.0280	0.88
Fine parenchyma/lung	0.8948 ± 0.0060	0.8900 ± 0.0255	0.76
Septum/lung	0.0894 ± 0.0087	0.1020 ± 0.0047	**0.03**
Total epithelium/septum	0.1611 ± 0.0033	0.1693 ± 0.0083	0.17
Type I epithelium/septum	0.0991 ± 0.0011	0.0994 ± 0.0040	0.88
Type II epithelium/septum	0.0620 ± 0.0037	0.0700 ± 0.0046	**0.03**
Interstitium/septum	0.1613 ± 0.0109	0.1677 ± 0.0014	0.13
Endothelium/septum	0.1113 ± 0.0034	0.1059 ± 0.0021	**0.01**
Extravascular tissue/septum	0.4337 ± 0.0143	0.4429 ± 0.0115	0.21
Capillary blood/septum	0.5663 ± 0.0143	0.5571 ± 0.0115	0.21
	Surface/volume ratio, cm^{-1}		
Alveoli/septum	3,856 ± 85	3,850 ± 80	0.88
Capillary/septum	4,222 ± 73	4,244 ± 87	0.44

Values are means ± SD; 4 animals/group. EPO, erythropoietin. *P* values <0.05 are shown in boldface.

DISCUSSION

Summary of the major findings. This study is novel in two ways: by *1*) establishing the feasibility of chronic inhalational delivery of an angiogenic growth factor in a large animal model and *2*) establishing the structural and functional effects of EPO delivery on post-PNX compensatory lung growth. We tested the hypothesis that inhalational delivery of EPO, a paracrine proangiogenic and growth-promoting protein known to be upregulated following PNX (9, 45, 47) enhances compensatory lung growth in a well-characterized adult canine model. Major findings are *1*) inhalation of EPO nanoparticles increased serum EPO concentration by 6%–13% with a mild change in systemic hematocrit; *2*) EPO inhalation abrogated post-PNX lipid oxidative stress measured by circulating 8-isoprostane level, consistent with the cytoprotective effect of EPO; *3*) EPO inhalation did not alter post-PNX lung function measured at rest; *4*) EPO treatment variably enhanced the volume densities of alveolar septum per unit of lung volume, alveolar type II epithelium per unit of septal tissue volume, and endothelium per unit of septal tissue volume in the remaining lobes; and *5*) EPO treatment significantly accentuated post-PNX increase in the prevalence of alveolar double capillaries. Results indicate that chronic inhalational EPO delivery reduced post-PNX oxidative stress damage, enhanced intussusceptive alveolar-capillary formation in all remaining lobes, and selectively accentuated growth of extravascular alveolar tissue constituents in some but not all remaining lobes. Owing to the regional heterogeneity of response, post-PNX whole-lung alveolar extravascular tissue growth and resting lung function were not enhanced above that in the control group.

Critique of the methods. The canine PNX model is extremely robust; we were able to repeatedly discern differences in key parameters using three to five animals per group (7, 32, 45). Even with a small number of animals (four per group), the physiological and morphometric response pattern was consistent between treatment groups. Bioactivity of EPO nanoparticles is evidenced in vitro by the rescue of EPO-dependent BaF3 cells overexpressing EPO receptor and in vivo by modest increases in serum EPO concentration, with a modestly larger post-PNX increase in circulating hemoglobin concentration measured under anesthesia but not while awake. The latter is likely due to splenic contraction under sympathetic stimulation releasing sequestered erythrocytes that masked the basal difference under anesthesia. Morphometric alveolar-capillary he-

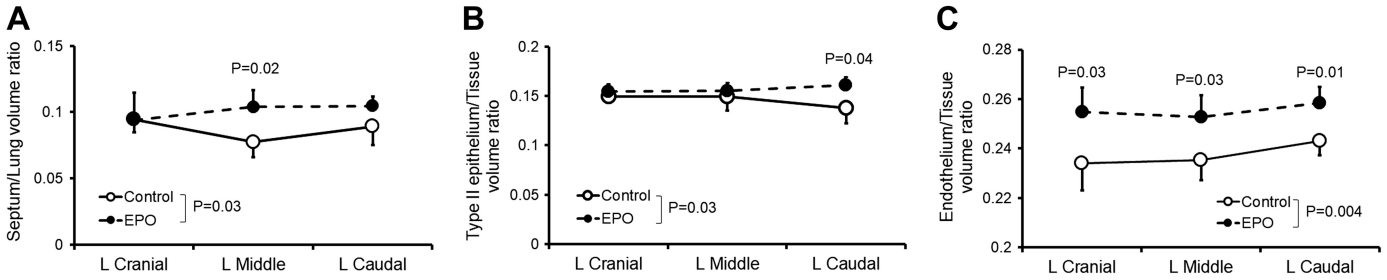


Fig. 7. Volume-to-volume ratios of septum per unit of lung volume (*A*), type II epithelium per unit of septal tissue volume (*B*), and endothelium per unit of tissue volume (*C*), in the post-PNX remaining lobes of control and EPO-treated animals ($n = 4$ animals each). Mean ± SD. *P* values indicate differences between treatment groups, by repeated measures ANOVA and post hoc Fisher's PLSD test. EPO, erythropoietin; L, left; PNX, pneumonectomy.

Downloaded from journals.physiology.org/journal/ajplung (193.140.001.200) on February 25, 2022.

Table 3. *Morphometry: absolute volumes and surface areas*

	Treatment		
	Control	EPO	*P* Value
	Volume, ml/kg		
Lung			
Intact	54.76 ± 9.13	51.99 ± 5.72	0.63
After sectioning	48.53 ± 10.03	45.88 ± 6.53	0.67
Septum	4.33 ± 0.98	4.67 ± 0.58	0.57
Total epithelium	0.70 ± 0.17	0.79 ± 0.07	0.38
Type I epithelium	0.43 ± 0.09	0.46 ± 0.04	0.52
Type II epithelium	0.27 ± 0.08	0.32 ± 0.03	0.25
Interstitium	0.70 ± 0.14	0.78 ± 0.09	0.36
Endothelium	0.48 ± 0.11	0.49 ± 0.05	0.86
Extravascular septal tissue	1.88 ± 0.42	2.06 ± 0.21	0.47
Capillary blood	2.45 ± 0.56	2.61 ± 0.37	0.66
	Surface area, m^2/kg		
Alveoli	1.67 ± 0.39	1.80 ± 0.24	0.60
Capillary	1.83 ± 0.44	1.98 ± 0.25	0.57

Values are means ± SD; 4 animals/group. EPO, erythropoietin.

matocrit was not different between groups, suggesting similar erythrocyte retention in the lung. Cellular actions of EPO were evidenced by the higher mitochondrial content within type II epithelial cell suggesting heightened cellular metabolic activity, the increased iron-containing inclusion bodies within interstitial cells suggesting iron mobilization, and the mitigation of post-PNX lipid oxidative stress damage, in EPO-treated animals. Duration of EPO treatment spanned the period of most active post-PNX alveolar-capillary cellular proliferation, although architectural remodeling, parenchymal relaxation, and improvement in gas exchange may continue beyond the treatment period (44). Comparisons of lung function measured in anesthetized animals and at postmortem may differ from that in conscious animals and during exertion.

Targeting EPO delivery to the lung minimizes drug waste and off-target effects associated with systemic administration. Recirculating the expired air via a rebreathing circuit helped maximizing drug delivery. Optimal dose of EPO is unknown. The weekly EPO dose (100 IU/kg) is at the lower end of the range given to correct anemia in patients with end-stage renal failure (40); this dose was well tolerated and sufficient to significantly raise serum EPO concentration with only a mild change in systemic hemoglobin concentration. We previously showed that using PLGA nanoparticles as carrier for inhalation delivery facilitates EPO uptake by lung cells, resulting in widespread EPO deposition in rat lung, which persist for up to 10 days after 1 dose (25). Similarly, EPO was well distributed in canine lung following inhalation (Fig. 3*A*). Repeated deliveries of PLGA, an FDA-approved biocompatible and biodegradable polymer, did not alter the metabolic panel measured in control animals (data not shown).

Signals and mediators of compensatory lung growth. In adult dogs following right PNX, the remaining lobes undergo accelerated compensatory growth with generation of new alveolar-capillary tissue and capillary constituents, followed by gradual acinar remodeling with tissue relaxation and alveolar septal thinning, eventually leading to significant improvement in lung mechanics and augmentation of alveolar gas exchange capacity of the remaining lobes (12, 15, 33). The major in vivo stimuli for compensatory alveolar-capillary growth are mechanical stress and deformation of the parenchyma and microvasculature resulting from lobar expansion and increased perfusion through the remaining lobes (7, 8, 32, 33). Endogenous compensatory lung growth involves balanced adaptation of all tissue-capillary components and coordination of nearly all major homeostatic metabolic pathways. Transcriptome analysis of murine lungs showed early post-PNX upregulation of genes involved in cell proliferation, extracellular matrix and protease components with a temporal pattern of initial dedifferentiation toward a more "primitive" state with greater proliferative potential followed by later redifferentiation (22). This pattern is consistent with our own observations in canines of early post-PNX generation of tissue and matrix elements accompanied by progressive architectural remodeling, with a post-PNX shift of alveolar-capillary profiles from the typical mature "single" to the immature "double" capillary morphology associated with new capillary formation via the process of intussusception (11).

Supplementation with growth promoters. In adult canines, post-PNX lung growth significantly enhances, but fails to completely normalize, structure-function of the remaining lung; this fact indicates retention of plasticity and suggests the possibility for exogenous interventions to augment the innate response. Approaches such as exposure to ambient hypoxia (37), systemic administration of epidermal growth factor (21), keratinocyte growth factor (KGF) (20) and retinoic acid (19), and exogenously enhanced expression of KGF (24) have been reported to modify post-PNX lung growth; however, none has been shown to augment alveolar gas exchange in the remaining lung. In adult canines, we found that supplementation with oral *all-trans* retinoic acid (RA) had little structural or functional effect following 42% lung resection where mechanical stimuli

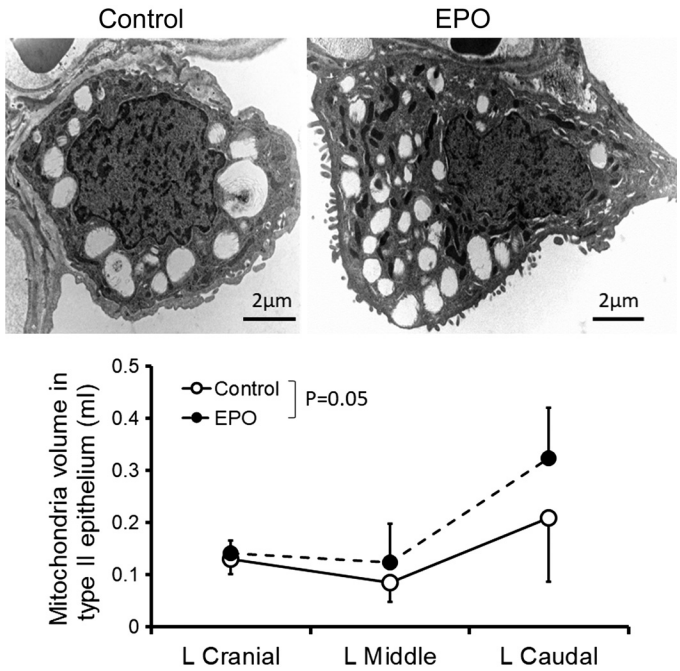


Fig. 8. Transmission electron micrographs and quantitative measurements show increased volumes of the electron-dense mitochondria within alveolar type II epithelium in post-PNX remaining lobes of EPO-treated compared with control animals (n = 4 animals each). Bar = 2 μm. Mean ± SD. *P* values indicate comparison between treatment groups by repeated measures ANOVA. EPO, erythropoietin; L, left; PNX, pneumonectomy.

Downloaded from journals.physiology.org/journal/ajplung (193.140.001.200) on February 25, 2022.

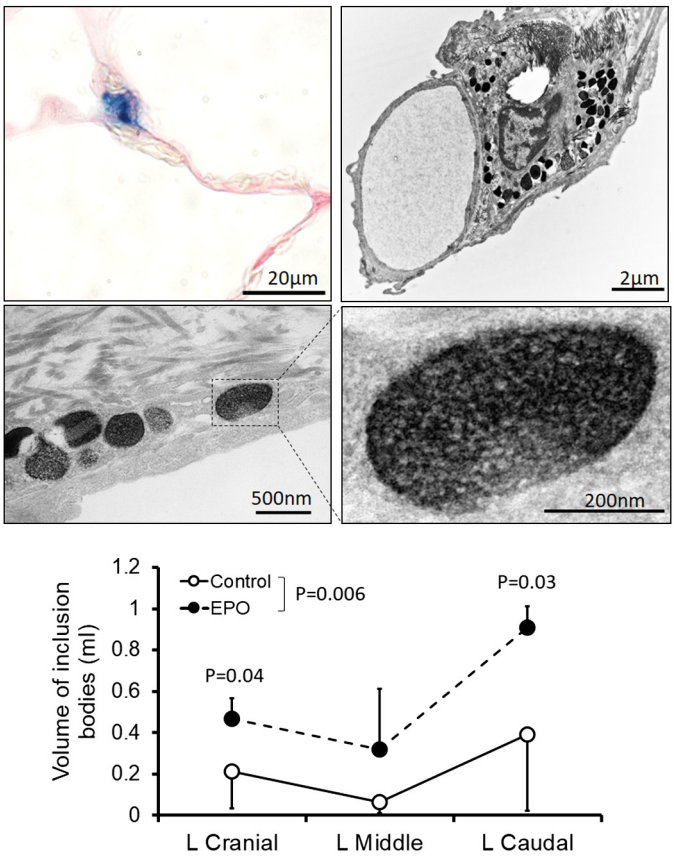


Fig. 9. Increased electron-dense inclusion bodies, consistent with ferritin-containing endosomes, were observed within interstitial cells in the post-PNX remaining lobes of EPO-treated compared with control animals (n = 4 each). *Top left*: light micrograph show foci of positive Prussian Blue stain for iron within the septum. *Top right and bottom*: electron micrographs of inclusion bodies are shown at increasing magnifications. *Inset*: one inclusion body was further magnified (lower right). *Bottom*: absolute volume (ml) of interstitial inclusion bodies in each remaining lobe. Mean ± SD. P values indicate comparison between treatment groups by repeated measures ANOVA and post hoc Fisher's protected least significant difference test. EPO, erythropoietin; L, left; PNX, pneumonectomy.

on the remaining lung fell below a growth-initiating threshold (41). In contrast, following 58% lung resection where mechanical stimuli exceeded a growth-initiating threshold, RA supplementation further increased the gain in extravascular alveolar tissue and double-capillary formation compared with vehicle-treated controls (42). These results support the interpretation that exogenous growth mediators may enhance active mechanically initiated lung growth but cannot initiate lung growth de novo in the absence of sufficient mechanical stimuli. Moreover, RA-stimulated alveolar tissue growth is nonuniform, with thickened septa and capillary basement membranes, small air spaces, and distorted acinar architecture, resulting in reduced lung compliance without enhancement of lung diffusing capacity or exercise performance compared with vehicle-treated controls (6, 30, 42). Thus, selective growth factor supplementation may lead to "unbalanced" response and structure-function discrepancy where the generation of new tissue and capillaries fails to further improve function of the remaining lung.

EPO inhalation. Alveolar angiogenesis, a critical process for post-PNX compensation, is initiated predominantly by mechanical signals associated with the redistribution of perfusion to the remaining lung. New capillaries form from existing ones via intussusception (3, 14). As more lung units are removed from 58% up to 70% of total, double-capillary formation in the remaining lobes continue to increase even as alveolar tissue growth reaches an upper limit (33), suggesting separate stimuli are responsible for parenchymal and capillary growth. Restricting the post-PNX increase in perfusion by selective lobar pulmonary artery banding leads to redistribution of pulmonary blood flow among the remaining lobes and impaired compensatory responses (8). The mechanosensitive HIF-1α-EPO-VEGF axis is coordinately upregulated in adult canine lungs following PNX, supporting its role in mediating compensatory responses (45, 46) and our rationale for testing EPO supplementation post-PNX. Our finding of EPO enhancement of post-PNX double-capillary formation is consistent with the known angiogenic actions of the EPO-EPOR axis. Although we observed lobe-specific enhancement of selected primary morphometric measurements (Fig. 7) there was no augmentation of whole-lung average alveolar septal tissue volume, lung volumes, or resting lung diffusing capacity. These results parallel our earlier findings using oral *all trans* retinoic acid supplementation that selectively augmented some but not all aspects of active post-PNX alveolar-capillary growth but failed to further enhance lung function (6, 30, 42). The structure-function discrepancy in response to pharmacological intervention is not entirely unexpected given the complex interactions of myriad genes and homeostatic pathways that are activated by post-PNX mechanical perturbation and the need for spatio-temporal coordination of their actions among disparate lobes of the remaining lung. It is evident that any single exogenous growth factor is insufficient to amplify endogenous post-PNX responses in a balanced manner; in fact, such a strategy may promote distorted or unbalanced responses that detract from overall structure-function compensation.

Compensatory versus pathological alveolar angiogenesis. Post-PNX alveolar angiogenesis shares many similar signals, pathways, and mediators (e.g., mechano-sensitivity, reactive oxygen species, HIF-1α-EPO-VEGF activation), with pathological flow-dependent angiogenesis in pulmonary vascular

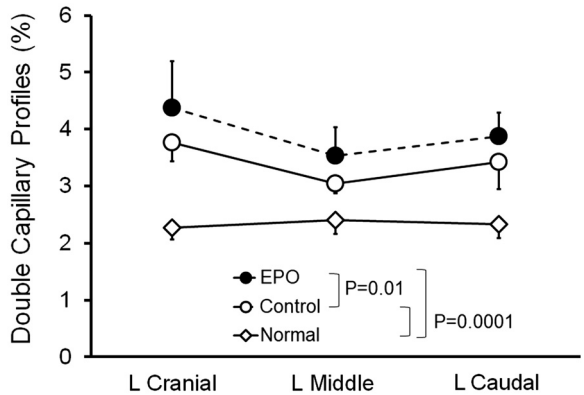


Fig. 10. Prevalence of double-capillary profiles (% of total capillary profiles) in post-PNX remaining lobes of the left (L) lung following EPO or control treatment (n = 4 animals each) compared with unoperated normal adult canines (n = 6) reported previously (33). Mean ± SD. P values indicate differences between groups for all lobes by repeated measures ANOVA. EPO, erythropoietin; PNX, pneumonectomy.

Downloaded from journals.physiology.org/journal/ajplung (193.140.001.200) on February 25, 2022.

disease, e.g., hepatopulmonary syndrome (29), pulmonary arterial hypertension (39), metastatic lung tumors (1); yet the functional end points are diametrically different. Our interventional studies using EPO or *all-trans* retinoic acid offer potential insight into the disparity. Post-PNX alveolar angiogenesis is synchronized with extravascular septal tissue growth and appropriate remodeling of acini and conducting bronchovasculature, leading to optimized mechanical properties, increased conductance of blood-gas barrier, and preserved ventilation-perfusion-diffusion matching. In contrast, pathological flow-induced angiogenesis is uncoordinated and desynchronized with respect to extravascular and extra-septal structures and physiological processes; skewed responses lead to mechanical dysfunction, inefficient alveolar-capillary diffusion, and ventilation-perfusion-diffusion mismatch. The magnitude, distribution, and duration of the inciting stimuli and their interaction with the microenvironment (e.g., inflammation, architectural distortion) modulate the ability to elicit and propagate balanced downstream responses via pre-programmed pathways and mediators that when differentially amplified throughout the whole lung, determine whether the outcome is adaptive or maladaptive.

Conclusions

We established the techniques, feasibility, and effectiveness of chronic inhalational delivery of a cytoprotective proangiogenic protein for modifying compensatory lung growth in a large animal model. Post-PNX inhalational EPO delivery significantly reduced lipid oxidative stress damage, variably and modestly augmented regional growth of selected alveolar tissue components, and significantly enhanced intussusceptive alveolar-capillary formation in all remaining lobes. Furthermore, we observed improved uniformity of in vivo pulmonary blood volume distribution in these EPO-treated animals assessed by serial volumetric computed tomography (Dane DM, Yilmaz C, Tustison N, Gee JC, Hsia CCW, unpublished observations). The aggregate findings indicate modest structural and physiologic enhancement in response to chronic EPO delivery. However, the selective and unbalanced lobar responses to a single growth promoter were insufficient to enhance overall alveolar tissue growth or resting gas exchange of the entire remaining lung. This structure-function dissociation in response to exogenous growth promoters constitutes a major challenge facing the field of regenerative pulmonary medicine; this challenge applies equally to other approaches such as cell-based regenerative therapy and bioengineered lungs. Future investigation might include use of combination or serial growth factors to target different lung structures and promote complementary aspects of compensatory lung growth, i.e., analogous to the "cocktail" chemotherapy regimens used in cancer treatment. It remains a major challenge to develop effective strategies to fully harness the innate plasticity of the mammalian lung.

ACKNOWLEDGMENTS

The authors thank Dr. Matthew Riegel, Angela Guillory, and the staff of the Animal Resources Center at University of Texas Southwestern Medical Center for excellent veterinary care. They also thank Khoa Cao, Yu-An Zhang, and the staff of the Electron Microscopy Core Facility at University of Texas Southwestern Medical Center for technical assistance.

GRANTS

This work was supported in part by National Institutes of Health National Heart, Lung and Blood Institute Grants U01 HL-111146, R01 HL-40070, and R01 HL-134373. The content of this manuscript is solely the authors' responsibility and does not necessarily represent the official views of the funding agency.

DISCLOSURES

No conflicts of interest, financial or otherwise, are declared by the authors.

AUTHOR CONTRIBUTIONS

C.C.W.H. conceived and designed research; D.M.D., C.Y., D.G., R.I., J.M., K.N., P.R., A.S.E., and C.C.W.H. performed experiments; D.M.D., C.Y., D.G., R.I., J.M., K.N., P.R., A.S.E., and C.C.W.H. analyzed data; D.M.D., C.Y., and C.C.W.H. interpreted results of experiments; D.M.D. and C.C.W.H. prepared figures; D.M.D. and C.C.W.H. drafted manuscript; C.C.H. edited and revised manuscript; D.M.D., C.Y., R.I., J.M., K.N., P.R., and C.C.W.H. approved final version of manuscript.

REFERENCES

1. **Bačić I, Karlo R, Zadro AS, Zadro Z, Skitarelić N, Antabak A.** Tumor angiogenesis as an important prognostic factor in advanced non-small cell lung cancer (Stage IIIA). *Oncol Lett* 15: 2335–2339, 2018. doi:10.3892/ol.2017.7576.
2. **Bartoli CR, Akiyama I, Okabe K, Diaz EA, Godleski JJ.** Permanent tracheostomy for long-term respiratory studies. *J Surg Res* 145: 124–129, 2008. doi:10.1016/j.jss.2007.03.076.
3. **Burri PH.** Structural aspects of postnatal lung development - alveolar formation and growth. *Biol Neonate* 89: 313–322, 2006. doi:10.1159/000092868.
4. **Chang H, Shyu KG, Wang BW, Kuan P.** Regulation of hypoxia-inducible factor-1alpha by cyclical mechanical stretch in rat vascular smooth muscle cells. *Clin Sci (Lond)* 105: 447–456, 2003. doi:10.1042/CS20030088.
5. **Dane DM, Johnson RL JR, Hsia CC.** Dysanaptic growth of conducting airways after pneumonectomy assessed by CT scan. *J Appl Physiol (1985)* 93: 1235–1242, 2002. doi:10.1152/japplphysiol.00970.2001.
6. **Dane DM, Yan X, Tamhane RM, Johnson RL JR, Estrera AS, Hogg DC, Hogg RT, Hsia CCW.** Retinoic acid-induced alveolar cellular growth does not improve function after right pneumonectomy. *J Appl Physiol (1985)* 96: 1090–1096, 2004. doi:10.1152/japplphysiol.00900.2002.
7. **Dane DM, Yilmaz C, Estrera AS, Hsia CC.** Separating in vivo mechanical stimuli for postpneumonectomy compensation: physiological assessment. *J Appl Physiol (1985)* 114: 99–106, 2013. doi:10.1152/japplphysiol.01213.2012.
8. **Dane DM, Yilmaz C, Gyawali D, Iyer R, Ravikumar P, Estrera AS, Hsia CC.** Perfusion-related stimuli for compensatory lung growth following pneumonectomy. *J Appl Physiol (1985)* 121: 312–323, 2016. doi:10.1152/japplphysiol.00297.2016.
9. **Foster DJ, Moe OW, Hsia CC.** Upregulation of erythropoietin receptor during postnatal and postpneumonectomy lung growth. *Am J Physiol Lung Cell Mol Physiol* 287: L1107–L1115, 2004. doi:10.1152/ajplung.00119.2004.
10. **Foster DJ, Ravikumar P, Bellotto DJ, Unger RH, Hsia CC.** Fatty diabetic lung: altered alveolar structure and surfactant protein expression. *Am J Physiol Lung Cell Mol Physiol* 298: L392–L403, 2010. doi:10.1152/ajplung.00041.2009.
11. **Hsia CC.** Comparative analysis of the mechanical signals in lung development and compensatory growth. *Cell Tissue Res* 367: 687–705, 2017. doi:10.1007/s00441-016-2558-8.
12. **Hsia CC, Herazo LF, Ramanathan M, Johnson RL JR, Wagner PD.** Cardiopulmonary adaptations to pneumonectomy in dogs. II. VA/Q relationships and microvascular recruitment. *J Appl Physiol (1985)* 74: 1299–1309, 1993. doi:10.1152/jappl.1993.74.3.1299.
13. **Hsia CC, Hyde DM, Ochs M, Weibel ER; ATS/ERS Joint Task Force on Quantitative Assessment of Lung Structure.** An official research policy statement of the American Thoracic Society/European Respiratory Society: standards for quantitative assessment of lung structure. *Am J Respir Crit Care Med* 181: 394–418, 2010. doi:10.1164/rccm.200809-1522ST.

Downloaded from journals.physiology.org/journal/ajplung (193.140.001.200) on February 25, 2022.

14. **Hsia CC, Ravikumar P.** Role of mechanical stress in lung repair and regeneration. In: *Stem cells in the Lung*, edited by Bertoncello I. Switzerland: Springer International, 2015, chapt 12, p. 191–212.
15. **Hsia CCW, Herazo LF, Fryder-Doffey F, Weibel ER.** Compensatory lung growth occurs in adult dogs after right pneumonectomy. *J Clin Invest* 94: 405–412, 1994. doi:10.1172/JCI117337.
16. **Ishaq M.** A morphological study of the lungs and bronchial tree of the dog: with a suggested system of nomenclature for bronchi. *J Anat* 131: 589–610, 1980.
17. **Jaquet K, Krause K, Tawakol-Khodai M, Geidel S, Kuck KH.** Erythropoietin and VEGF exhibit equal angiogenic potential. *Microvasc Res* 64: 326–333, 2002. doi:10.1006/mvre.2002.2426.
18. **Jelkmann W, Bohlius J, Hallek M, Sytkowski AJ.** The erythropoietin receptor in normal and cancer tissues. *Crit Rev Oncol Hematol* 67: 39–61, 2008. doi:10.1016/j.critrevonc.2008.03.006.
19. **Kaza AK, Kron IL, Kern JA, Long SM, Fiser SM, Nguyen RP, Tribble CG, Laubach VE.** Retinoic acid enhances lung growth after pneumonectomy. *Ann Thorac Surg* 71: 1645–1650, 2001. doi:10.1016/S0003-4975(01)02478-X.
20. **Kaza AK, Kron IL, Leuwerke SM, Tribble CG, Laubach VE.** Keratinocyte growth factor enhances post-pneumonectomy lung growth by alveolar proliferation. *Circulation* 106, *Suppl* 1: I120–I124, 2002.
21. **Kaza AK, Laubach VE, Kern JA, Long SM, Fiser SM, Tepper JA, Nguyen RP, Shockey KS, Tribble CG, Kron IL.** Epidermal growth factor augments postpneumonectomy lung growth. *J Thorac Cardiovasc Surg* 120: 916–921, 2000. doi:10.1067/mtc.2000.110460.
22. **Kho AT, Liu K, Visner G, Martin T, Boudreault F.** Identification of dedifferentiation and redevelopment phases during postpneumonectomy lung growth. *Am J Physiol Lung Cell Mol Physiol* 305: L542–L554, 2013. doi:10.1152/ajplung.00403.2012.
23. **Lasocki S, Millot S, Andrieu V, Lettéron P, Pilard N, Muzeau F, Thibaudeau O, Montravers P, Beaumont C.** Phlebotomies or erythropoietin injections allow mobilization of iron stores in a mouse model mimicking intensive care anemia. *Crit Care Med* 36: 2388–2394, 2008. doi:10.1097/CCM.0b013e31818103b9.
24. **Matsumoto K, Nagayasu T, Hishikawa Y, Tagawa T, Yamayoshi T, Abo T, Tobinaga S, Furukawa K, Koji T.** Keratinocyte growth factor accelerates compensatory growth in the remaining lung after trilobectomy in rats. *J Thorac Cardiovasc Surg* 137: 1499–1507, 2009. doi:10.1016/j.jtcvs.2008.11.037.
25. **Menon JU, Ravikumar P, Pise A, Gyawali D, Hsia CC, Nguyen KT.** Polymeric nanoparticles for pulmonary protein and DNA delivery. *Acta Biomater* 10: 2643–2652, 2014. doi:10.1016/j.actbio.2014.01.033.
26. **Mulcahy L.** The erythropoietin receptor. *Semin Oncol* 28, *Suppl* 8: 19–23, 2001. doi:10.1016/S0093-7754(01)90208-8.
27. **Pengelly LD.** Curve-fitting analysis of pressure-volume characteristics of the lungs. *J Appl Physiol Respir Environ Exerc Physiol* 42: 111–116, 1977. doi:10.1152/jappl.1977.42.1.111.
28. **Pufe T, Lemke A, Kurz B, Petersen W, Tillmann B, Grodzinsky AJ, Mentlein R.** Mechanical overload induces VEGF in cartilage discs via hypoxia-inducible factor. *Am J Pathol* 164: 185–192, 2004. doi:10.1016/S0002-9440(10)63109-4.
29. **Raevens S, Geerts A, Paridaens A, Lefere S, Verhelst X, Hoorens A, Van Dorpe J, Maes T, Bracke KR, Casteleyn C, Jonckx B, Horvatits T, Fuhrmann V, Van Vlierberghe H, Van Steenkiste C, Devisscher L, Colle I.** Placental growth factor inhibition targets pulmonary angiogenesis and represents a therapy for hepatopulmonary syndrome in mice. *Hepatology* 68: 634–651, 2018. doi:10.1002/hep.29579.
30. **Ravikumar P, Dane DM, McDonough P, Yilmaz C, Estrera AS, Hsia CC.** Long-term post-pneumonectomy pulmonary adaptation following all-trans-retinoic acid supplementation. *J Appl Physiol (1985)* 110: 764–773, 2011. doi:10.1152/japplphysiol.00994.2010.
31. **Ravikumar P, Menon JU, Punnakitikashem P, Gyawali D, Togao O, Takahashi M, Zhang J, Ye J, Moe OW, Nguyen KT, Hsia CCW.** Nanoparticle facilitated inhalational delivery of erythropoietin receptor cDNA protects against hyperoxic lung injury. *Nanomedicine (Lond)* 12: 811–821, 2016. doi:10.1016/j.nano.2015.10.004.
32. **Ravikumar P, Yilmaz C, Bellotto DJ, Dane DM, Estrera AS, Hsia CC.** Separating in vivo mechanical stimuli for postpneumonectomy compensation: imaging and ultrastructural assessment. *J Appl Physiol (1985)* 114: 961–970, 2013. doi:10.1152/japplphysiol.01394.2012.
33. **Ravikumar P, Yilmaz C, Dane DM, Bellotto DJ, Estrera AS, Hsia CC.** Defining a stimuli-response relationship in compensatory lung growth following major resection. *J Appl Physiol (1985)* 116: 816–824, 2014. doi:10.1152/japplphysiol.01291.2013.
34. **Ravikumar P, Yilmaz C, Dane DM, Johnson RL JR, Estrera AS, Hsia CC.** Developmental signals do not further accentuate nonuniform postpneumonectomy compensatory lung growth. *J Appl Physiol (1985)* 102: 1170–1177, 2007. doi:10.1152/japplphysiol.00520.2006.
35. **Richmond TD, Chohan M, Barber DL.** Turning cells red: signal transduction mediated by erythropoietin. *Trends Cell Biol* 15: 146–155, 2005. doi:10.1016/j.tcb.2005.01.007.
36. **Salazar E, Knowles JH.** An analysis of pressure-volume characteristics of the lungs. *J Appl Physiol* 19: 97–104, 1964. doi:10.1152/jappl.1964.19.1.97.
37. **Sekhon HS, Smith C, Thurlbeck WM.** Effect of hypoxia and hyperoxia on postpneumonectomy compensatory lung growth. *Exp Lung Res* 19: 519–532, 1993. doi:10.3109/01902149309031725.
38. **Srai SK, Chung B, Marks J, Pourvali K, Solanky N, Rapisarda C, Chaston TB, Hanif R, Unwin RJ, Debnam ES, Sharp PA.** Erythropoietin regulates intestinal iron absorption in a rat model of chronic renal failure. *Kidney Int* 78: 660–667, 2010. doi:10.1038/ki.2010.217.
39. **Voelkel NF, Gomez-Arroyo J.** The role of vascular endothelial growth factor in pulmonary arterial hypertension. The angiogenesis paradox. *Am J Respir Cell Mol Biol* 51: 474–484, 2014. doi:10.1165/rcmb.2014-0045TR.
40. **Wright DG, Wright EC, Narva AS, Noguchi CT, Eggers PW.** Association of erythropoietin dose and route of administration with clinical outcomes for patients on hemodialysis in the United States. *Clin J Am Soc Nephrol* 10: 1822–1830, 2015. doi:10.2215/CJN.01590215.
41. **Yan X, Bellotto DJ, Dane DM, Elmore RG, Johnson RL JR, Estrera AS, Hsia CC.** Lack of response to all-trans retinoic acid supplementation in adult dogs following left pneumonectomy. *J Appl Physiol (1985)* 99: 1681–1688, 2005. doi:10.1152/japplphysiol.00553.2005.
42. **Yan X, Bellotto DJ, Foster DJ, Johnson RL JR, Hagler HK, Estrera AS, Hsia CC.** Retinoic acid induces nonuniform alveolar septal growth after right pneumonectomy. *J Appl Physiol (1985)* 96: 1080–1089, 2004. doi:10.1152/japplphysiol.00771.2003.
43. **Yan X, Polo Carbayo JJ, Weibel ER, Hsia CC.** Variation of lung volume after fixation when measured by immersion or Cavalieri method. *Am J Physiol Lung Cell Mol Physiol* 284: L242–L245, 2003. doi:10.1152/ajplung.00184.2002.
44. **Yilmaz C, Tustison NJ, Dane DM, Ravikumar P, Takahashi M, Gee JC, Hsia CC.** Progressive adaptation in regional parenchyma mechanics following extensive lung resection assessed by functional computed tomography. *J Appl Physiol (1985)* 111: 1150–1158, 2011. doi:10.1152/japplphysiol.00527.2011.
45. **Zhang Q, Bellotto DJ, Ravikumar P, Moe OW, Hogg RT, Hogg DC, Estrera AS, Johnson RL JR, Hsia CC.** Postpneumonectomy lung expansion elicits hypoxia-inducible factor-1alpha signaling. *Am J Physiol Lung Cell Mol Physiol* 293: L497–L504, 2007. doi:10.1152/ajplung.00393.2006.
46. **Zhang Q, Moe OW, Garcia JA, Hsia CC.** Regulated expression of hypoxia-inducible factors during postnatal and postpneumonectomy lung growth. *Am J Physiol Lung Cell Mol Physiol* 290: L880–L889, 2006. doi:10.1152/ajplung.00213.2005.
47. **Zhang Q, Zhang J, Moe OW, Hsia CC.** Synergistic upregulation of erythropoietin receptor (EPO-R) expression by sense and antisense EPO-R transcripts in the canine lung. *Proc Natl Acad Sci USA* 105: 7612–7617, 2008. doi:10.1073/pnas.0802467105.

Downloaded from journals.physiology.org/journal/ajplung (193.140.001.200) on February 25, 2022.